devices. That scheme is more practially realizable than the first scheme, and offers the added advantage of not needing isolation resistors in the power combiner, and hence, it has no problems of power dissipation that would occur when such resistors are used.

ACKNOWLEDGMENT

The author thanks Dr. James W. Gewartowski of Bell Laboratories, and all of the MTT reviewers for useful comments and suggestions.

REFERENCES

[1] E. J. Wilkinson, "An *N*-Way Hybrid Power Divider," *IRE Trans. Microwave Theory Tech.*, vol. MTT-8, pp. 116–118, Jan., 1960.

[2] J. M. Schellenberg and M. Cohn, "A Wideband Radial Power Combiner for FET Amplifiers," *1978 IEEE Int. Solid-State Circuit Conf. Dig.*, Feb., 1978, pp. 164–165, 273.

[3] M. Cohn, B. D. Geller, and J. M. Schllenberg, "A 10-Watt Broadband FET Combiner/Amplifier," *1979 IEEE MTT-S Int. Microwave Symp. Dig.*, April, 1979 pp. 292–297.

[4] A. A. M. Saleh, "Planar, Electrically-Symmetric, N-Way, Hybrid Power Dividers/Combiners," *IEEE Trans. Microwave Theory Tech.*, vol. MTT-28, pp. 555–563, June 1980.

[5] Z. Galani and S. J. Temple, "A Broadband *N*-Way Combiner/Divider," *1977 IEEE MTT-S Int. Microwave Symp. Dig.*," June, 1977, pp. 499–502.

[6] N. Nagai, E. Maekaura, and K. Ono, "New *n*-Way Hybrid Power Dividers," *1977 IEEE MTT-S Int. Microwave Symp. Dig.*, June 1977, pp. 503–504.

[7] R. L. Ernst, R. L. Camisa, and A. Presser, "Graceful Degradation Properties of Matched *n*-Port Power Amplifier Combiners," *1977 IEEE MTT-S Int. Microwave Symp. Dig.*, June 1977, pp. 174–177.

Theoretical Investigations of TRAPATT Amplifier Operation

RICHARD K. MAINS, MEMBER, IEEE, N. A. MASNARI, SENIOR MEMBER, IEEE, AND GEORGE I. HADDAD, FELLOW, IEEE

***Abstract*—A device–circuit interaction program has been developed for the study of TRAPATT amplifiers. The device is simulated using the programs developed by Bauhahn [1]. A slug-tuned coaxial circuit is simulated with the circuit parameters chosen to model an amplifier for which experimental results have previously been published [2]. Results including diode waveforms over the entire amplifier frequency band are presented. Separate mechanisms have been identified as being responsible for the fall off in gain and power output above and below the center frequency. The maximum bandwidth which can be attained with a TRAPATT amplifier is also estimated.**

I. INTRODUCTION

THE TRAPATT MODE was discovered by Prager *et al.* [3] in 1967. In 1970, detailed experimental results for a TRAPATT amplifier were published by Prager *et al.* [4]. Since that time, various workers have reported amplification in slug-tuned coaxial circuits [2], microstrip stagger-tuned circuits [5], [6], and coupled-line circuits [7], [8]. Typically, operation up to *X*-band has been achieved with gains of the order of 10 dB and maximum bandwidths of approximately 10 percent.

Manuscript received February 5, 1980; revised June 6, 1980. This work was supported by the U.S. Army Research Office.

R. Mains and G. I. Haddad are with the Electron Physics Laboratory, Department of Electrical and Computer Engineering, The University of Michigan, Ann Arbor, MI 48109.

N. A. Masnari is with the Department of Electrical Engineering, North Carolina State University, Raleigh, NC 27650.

A comprehensive theory explaining the experimental results of TRAPATT amplifiers has not been presented. A theoretical analysis of the TRAPATT device is difficult for several reasons. The complexity of TRAPATT operation severely limits the applicability of simplified analyses and necessitates a full device simulation, especially for the amplifier case where variations in the diode waveforms due to complex device–circuit interactions occur throughout the frequency band of operation. Even with a full simulation, it is believed that many sets of device waveforms and modes of TRAPATT amplification are possible depending upon the diode-circuit parameters. The choice of a particular configuration for a device–circuit interaction prevents the analysis from being a general one. The problem is further complicated by the nonperiodicity of the calculated TRAPATT waveforms. Nevertheless, it is believed that the analysis of simulation results for particular configurations can reveal certain aspects of the TRAPATT amplifier which are of general utility.

II. DEVICE PROGRAM

The simulation proceeds in the time domain. The TRAPATT diode simulation requires programs [1] which perform the following function from the terminal point of view: given the state of the diode at a particular time t

0018-9480/80/1000-1070$00.75

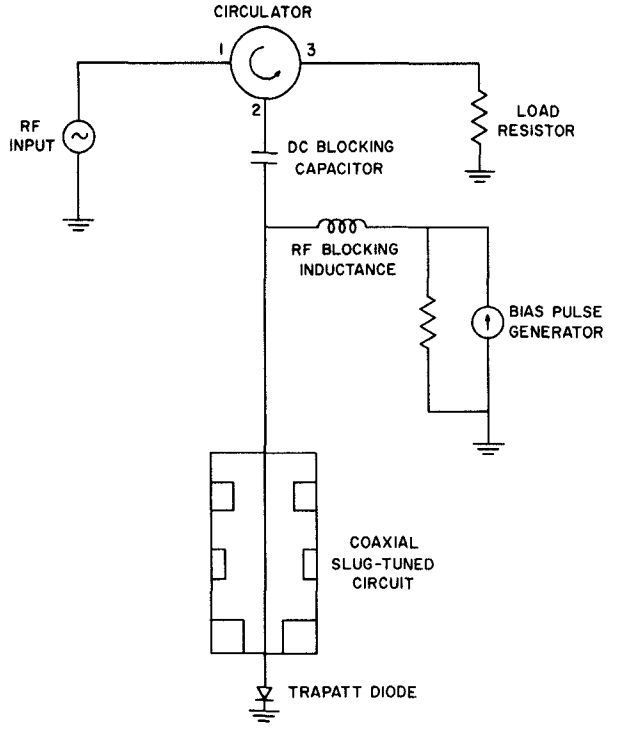

Fig. 1. Reflection amplifier circuit.

TABLE I
METHOD OF SOLUTION USED IN THE DIODE SIMULATION

1. $$q\frac{\partial p}{\partial t} = G[E(x,t)] - \frac{\partial J_p(x,t)}{\partial x} \quad (A)$$
$$q\frac{\partial n}{\partial t} = G[E(x,t)] + \frac{\partial J_n(x,t)}{\partial x} \quad (B)$$
yields $p(t+\Delta t)$, $n(t+\Delta t)$.

2. $$\varepsilon\frac{\partial E(t+\Delta t)}{\partial x} = q[p(x,t+\Delta t) - n(x,t+\Delta t) - N_A^-(x)]$$
subject to: $$V_T(t+\Delta t) = \int_0^W E(t+\Delta t)\,dx$$
yields $E(t+\Delta t)$

3. $$v_{p,n}(t+\Delta t,x) = v_{ps,ns}\left\{1 - \exp\left[-E(x,t+\Delta t)u_{p,n}/v_{ps,ns}\right]\right\}$$
yields $v_{p,n}(t+\Delta t,x)$

4. $$J_p(x,t+\Delta t) = qp(x,t+\Delta t)v_p(x,t+\Delta t) - qD_p\frac{\partial p(t+\Delta t)}{\partial x}$$
$$J_n(x,t+\Delta t) = qn(x,t+\Delta t)v_n(x,t+\Delta t) + qD_n\frac{\partial n(t+\Delta t)}{\partial x}$$
$$J_{tot}^{(t+\Delta t)} = \frac{1}{W}\int_0^W [J_p(t+\Delta t) + J_n(t+\Delta t)]\,dx$$
yields $J_{p,n}(x,t+\Delta t)$

5. $$G[E(x,t+\Delta t)] = A_p \exp[-B_p/E(x,t+\Delta t)]|J_p(x,t+\Delta t)| + A_n \exp[-B_n/E(x,t+\Delta t)]|J_n(x,t+\Delta t)|$$

and given the terminal voltage impressed at $t+\Delta t$, the resulting terminal current and new diode state is determined at $t+\Delta t$. The method of solution is illustrated in Table I. The device is divided into a uniform, one-dimensional mesh in space. It is assumed that the diode state is completely known at time t. Step 1 allows determination of the electron and hole concentrations, $n(t+\Delta t)$ cm^{-3} and $p(t+\Delta t)$ cm^{-3}, using the continuity equation with the previously determined generation term $G(\text{C}\cdot\text{s}^{-1}\cdot\text{cm}^{-3})$ and particle currents J_p, $J_n(\text{A}\cdot\text{cm}^{-2})$. In Step 2 the electric field $E(t+\Delta t)(\text{V}\cdot\text{cm}^{-1})$ is determined from Gauss' law and the imposed terminal voltage $V_T(t+\Delta t)$; here it is assumed that the semiconductor is p-type with acceptor concentration N_A^- cm^{-3}. In Step 3 the particle velocities at $t+\Delta t$ are calculated from the new electric field and the material parameters. Enough is known at this stage to calculate the particle current densities and the total induced current $J_{tot}(\text{A}\cdot\text{cm}^{-2})$ at $t+\Delta t$ in Step 4. Finally, the generation rate at $t+\Delta t$ is calculated in Step 5. At this point the diode is completely specified at $t+\Delta t$, and the process advances by another time step.

III. Circuit Program

A slug-tuned coaxial TRAPATT amplifier was simulated with circuit parameters selected to model an amplifier reported by Hughes [2]. Fig. 1 illustrates the configuration of the amplifier. The input to be amplified is coupled by a circulator to the coaxial line. The diode bias is introduced through a bias network. The reflected RF signal is channeled by the circulator to the load resistor.

The complete circuit model used in the program is shown in Fig. 2. The transmission-line section consists of three tuning slugs with characteristic impedances Z_1, Z_2, and Z_3. A lumped-element network attached to the left-hand side of the coaxial line models the diode package and mounting parasitics; this lumped-element network is interfaced with the device simulation described previously. Lumped elements are attached on the right-hand side of the coaxial line to model the bias network and the circulator of Fig. 1. The bias current I_B is assumed to have a linear rise characteristic until it reaches a prescribed constant value. The RF input signal is introduced as a traveling wave at point P moving toward the diode.

To simulate the coaxial line, the propagation of the forward- and reverse-traveling waves is calculated, as well as the reflections at impedance discontinuities and at the left- and right-hand extremities of the line. The efficiency of the simulation is greatly increased by considering the traveling waves as fixed and the coaxial line as moving, a technique developed by Khochnevis-Rad [9]. In this manner, unnecessary shifting operations are avoided at each time step.

The coupling between the coaxial line and the lumped-element networks is illustrated in Fig. 3. In Fig. 3(a), the incident and reflected voltage waves, f^- and f^+, are shown at the interface. The transmission line is replaced

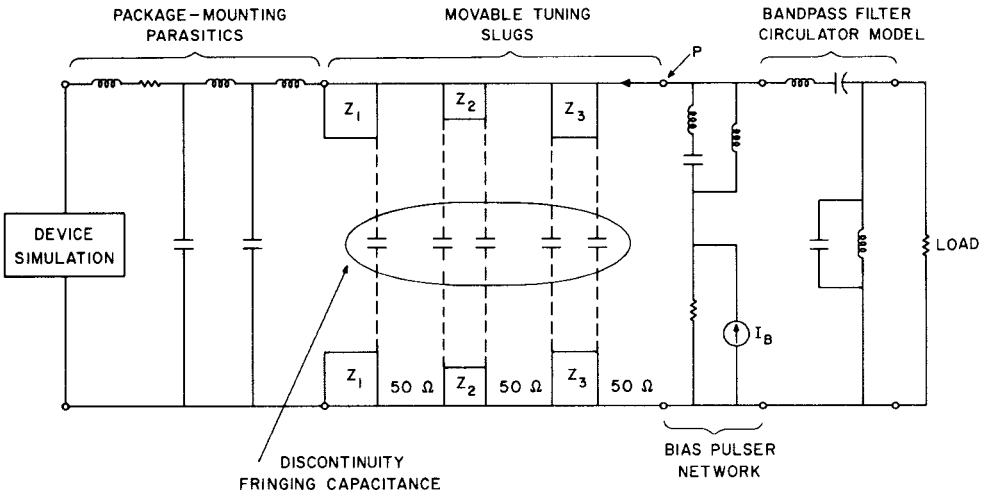

Fig. 2. Complete reflection amplifier circuit model.

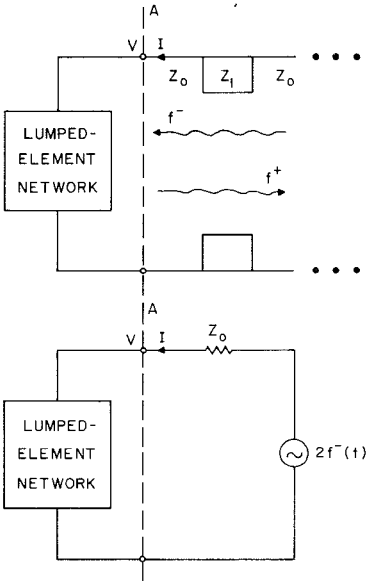

Fig. 3. Method of coupling between the coaxial line and a lumped-element network.

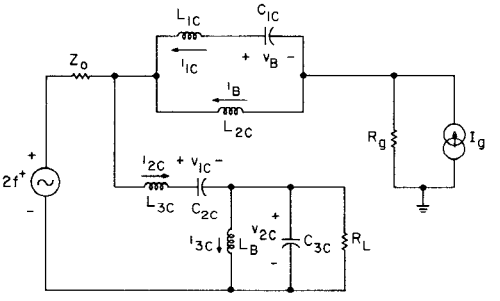

Fig. 4. Lumped elements representing the bias circuit, circulator, and load.

by a Thevenin equivalent voltage generator of value $2f^-$ V and characteristic impedance Z_0 in Fig. 3(b).

The method of solution of the lumped-element networks is the state-variable technique [10]. Fig. 4 shows the bias-circulator-load lumped-element networks. The voltage generator and impedance Z_0 are the Thevenin equivalent of the transmission line. The state variables are chosen to be the capacitor voltages and the inductor currents. For each state variable, one first-order differential equation can be written. The differential equations are converted to finite-difference equations using the trapezoidal rule. The resulting equations are solved for the state

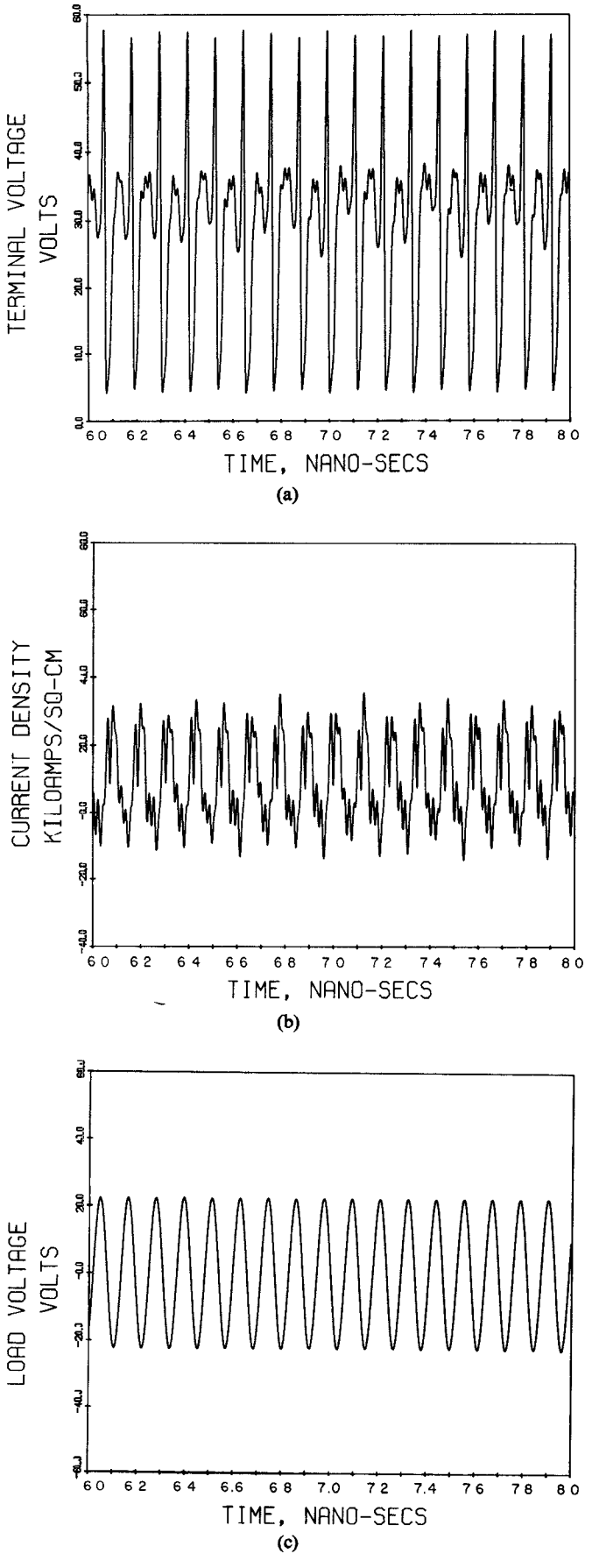

Fig. 5. (a) Diode terminal voltage. (b) Current density. (c) Load voltage. ($f_0 = 8.6$ GHz, $V_{RF} = 12.19$ V).

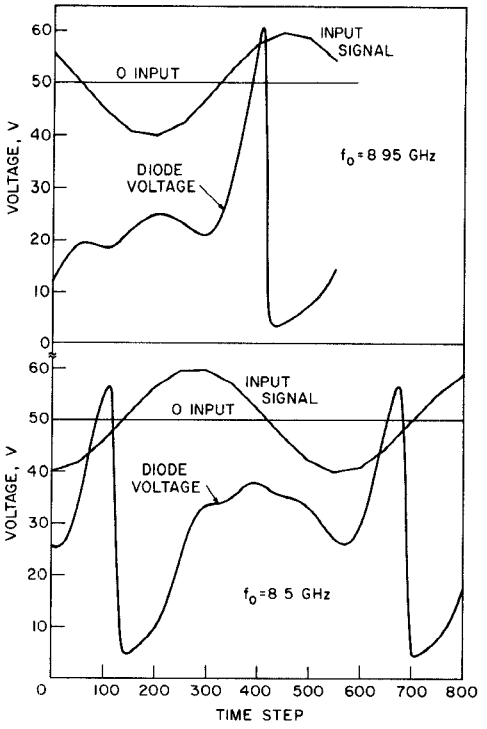

Fig. 6. Diode-voltage waveforms and corresponding input signal at the diode for two different operating frequencies.

variables at the future time, given their values at the present time and the future value of the voltage generator.

IV. Device–Circuit Interaction Results

At $t = 0$, a sinusoidal RF input is applied at point P in Fig. 2; also the bias current ramp I_B is turned on. The device waveforms and load voltage are observed until a stationary state has been reached. Fig. 5 shows a) the diode voltage, b) the current density, and c) the load voltage for an input frequency of 8.6 GHz and RF voltage amplitude of 12.19 V (based on a 50-Ω characteristic impedance). In this context, "stationary state" means that the time between voltage peaks for any two successive cycles in Fig. 5(a) varies within a narrow range about a clearly definable average value. In the cases considered here the variation was limited to approximately 5 percent. The resulting gain was 5.1 dB and the efficiency was 22 percent, comparing quite well with the experimental results being modeled [2] of 5-dB maximum gain and 18-percent efficiency at 8.73 GHz. Solutions were obtained over the entire frequency band, from 8.35 to 8.95 GHz; Fig. 6 shows device voltage waveforms obtained at input frequencies of 8.95 and 8.5 GHz, respectively. Also shown is the input signal at the diode terminals. It is apparent that, for different input frequencies, the relative phase established between the diode waveforms and the input signal varies. At higher input frequencies, the efficiency decreases because the diode voltage during the recovery portion of the cycle is lower. This is the mechanism responsible for decreased output power above the amplifier center frequency.

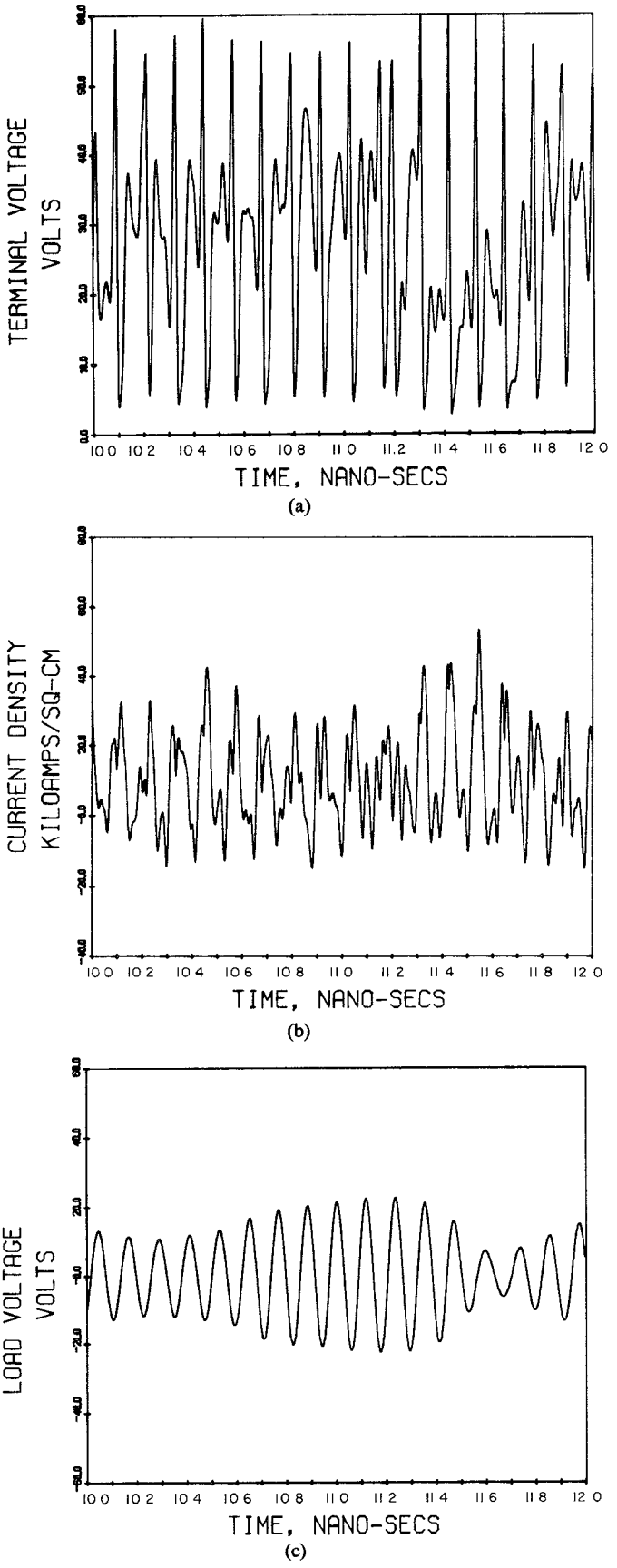

Fig. 7. (a), (b) Device waveforms. (c) Load voltage. The diode is not locked with the input. ($f=8.35$ GHz, $V_{RF}=12.19$ V, $I_B=1.568$ A).

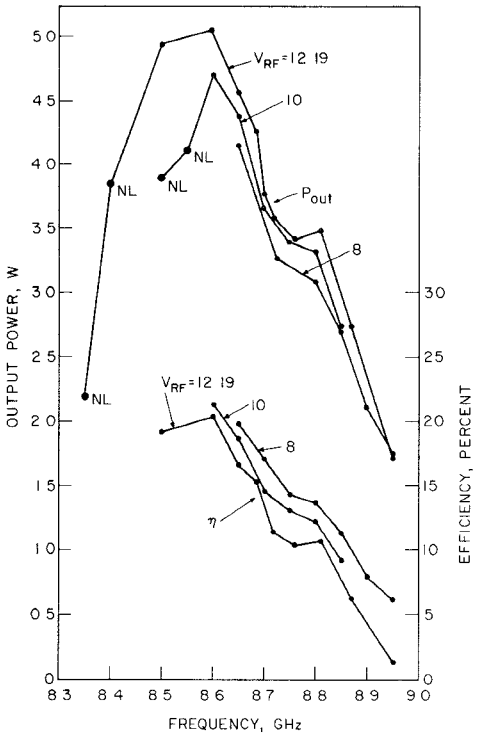

Fig. 8. Output power and fundamental efficiency versus frequency for $I_B=1.568$ A and various input levels.

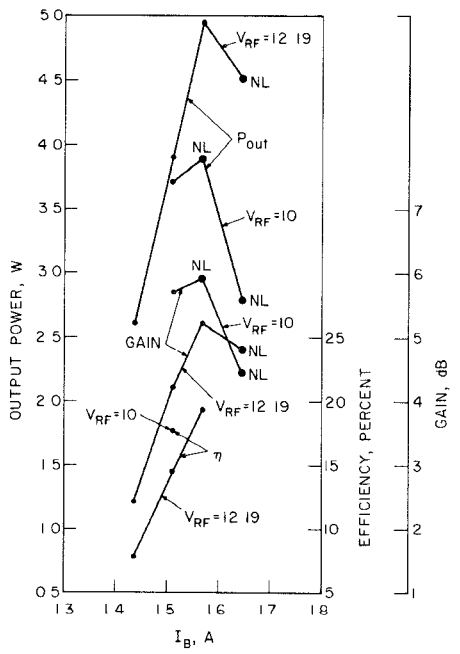

Fig. 9. Output power, gain and efficiency versus bias current I_B for $f_0=8.5$ GHz and two different input power levels.

Fig. 7 shows results at the low-frequency end, 8.35 GHz. It is seen that the diode waveforms do not remain in synchronism with the input; the average load power decreases from that of Fig. 5(c) due to low-frequency modulation thus identifying instability as the mechanism which

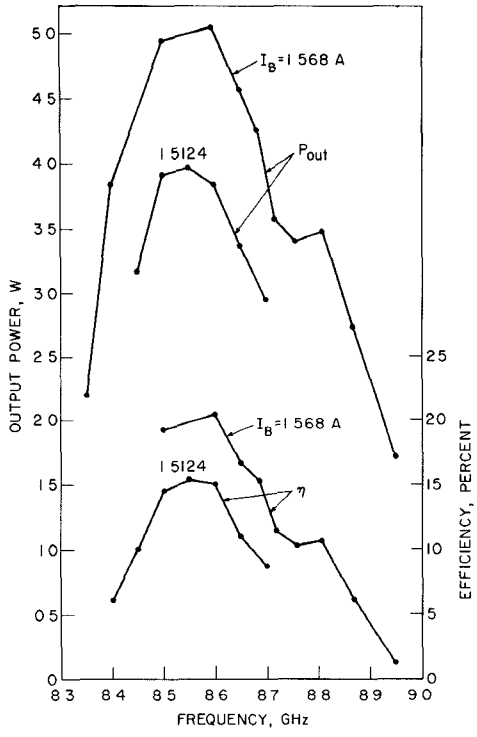

Fig. 10. Output power and efficiency versus frequency for $V_{RF}=12.19$ V and two different bias current levels.

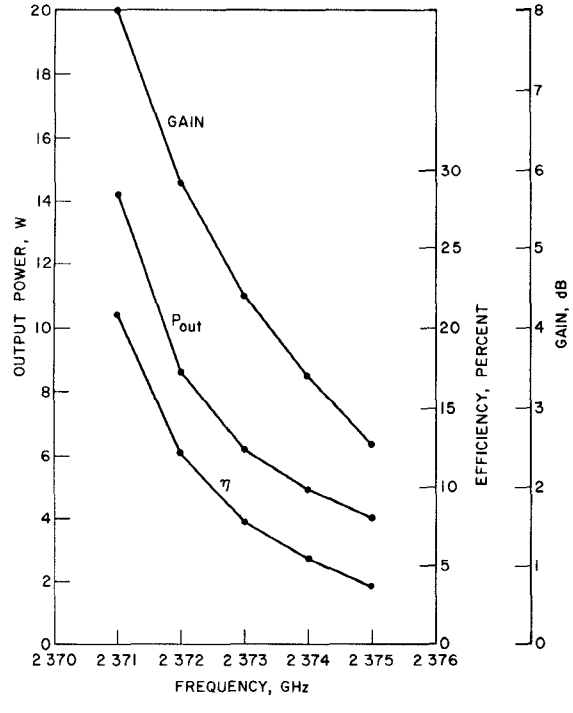

Fig. 11. Gain, output power, and efficiency for the narrow-band locked oscillator.

produces gain reduction at frequencies below the center frequency.

Simulations were carried out for different values of RF input voltage. Fig. 8 shows the resulting output power and efficiency versus input frequency. In these curves, "NL" indicates that a solution was unstable or not locked, as in Fig. 7.

Fig. 9 presents output power, gain and efficiency variations with bias current I_B at a constant input frequency of 8.5 GHz and with varying input amplitudes. The results indicate that the performance of the diode is very sensitive to the value of bias current with a value of 1.57 A yielding optimum output power. If the bias is increased beyond this value, the average output power decreases due to instabilities.

In Fig. 10, the output power and efficiency versus frequency are shown for two different values of bias current I_B. For $I_B=1.568$ A, the TRAPATT was found to operate as a locked oscillator, because the device produced output power in the absence of any input RF signal. For $I_B=1.5124$ A, the device behaved as a true amplifier; i.e., if the simulation was carried out with no input signal, no output power was produced.

A narrow-band locked oscillator at *S*-band [9] was also simulated. Fig. 11 shows the resulting gain, output power, and efficiency for this case. It was difficult to simulate operation below 2.371 GHz because the resulting waveforms were unstable. To investigate why this circuit is narrow band while the previous circuit yielded broad-band amplification, the impedance versus frequency presented at the diode terminals was calculated for both cases. Fig. 12 shows the impedance for the narrow-band locked oscillator, and Fig. 13 presents the impedance for the broad-band circuit. In both figures, f_0 is the frequency of maximum output power.

The diode area for the narrow-band simulations was larger than the area of the diode used with the broad-band circuit; therefore, it is expected that the impedance levels in Fig. 12 should be lower than for Fig. 13. The ratio of fundamental impedance values for these two cases is approximately equal to this area ratio. In the second-harmonic band, it is seen that the reactance slope is steeper for the broad-band case shown in Fig. 13. It might intuitively be expected that a smaller reactance slope would yield a broader bandwidth; however, the results of these simulations have shown that a steep second-harmonic reactance slope is required. Published experimental results [8] of TRAPATT amplifier impedance versus frequency characteristics show a sharp resonance at the low end of the second-harmonic band. However, this is not conclusive because other published results [11] indicate that minimizing the reactance slope favors broad bandwidth operation.

If however it is hypothesized that, at least for the type of slug-tuned coaxial circuit used in these simulations, the reactance slope in Fig. 12 is too small to achieve broad-band TRAPATT amplification, an estimate of the maximum attainable bandwidth for a TRAPATT amplifier is obtained. If the resonant frequency occurring approximately at 4 GHz in Fig. 12 were moved to the right by suitable circuit adjustment, keeping the value of imped-

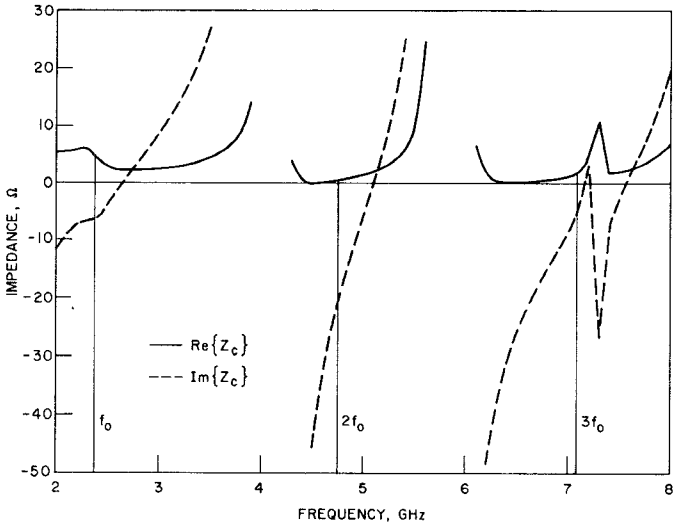

Fig. 12. Frequency dependence of the circuit impedance presented the diode terminals for the narrow-band locked oscillator.

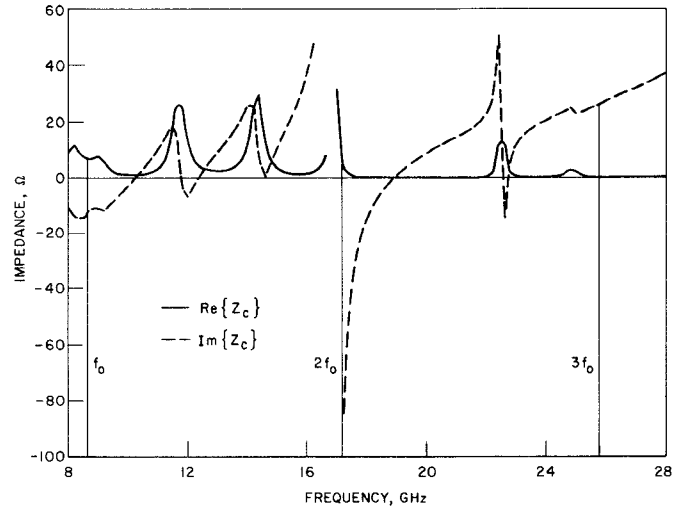

Fig. 13. Impedance presented at the diode terminals for the Hughes circuit.

ance constant at $2f_0$, a point would be reached where the reactance slope would be optimum for broad-band amplification. At this point, the stable fundamental bandwidth is given by half the separation between $2f_0$ and the second-harmonic resonant frequency of the circuit. This bandwidth will be less than half the frequency separation in Fig. 12. Calculating half the frequency interval between the circuit resonance and $2f_0$ in Fig. 12 yields a maximum achievable bandwidth of approximately 15 percent for a TRAPATT amplifier.

V. Conclusions

The TRAPATT device is inherently a large-signal multifrequency device. To realistically model TRAPATT amplifier operation, a comprehensive circuit program was developed which adequately models the experimentally obtained characteristics of an amplifier circuit in all the important frequency ranges. The TRAPATT device was simulated using a one-dimensional finite-difference algorithm which includes the variation of particle velocities and ionization rates with electric field. By coupling these two programs, device–circuit interactions in the time domain were carried out for many combinations of circuit parameters, RF drive, and diode bias. It was shown how the resulting diode waveforms vary over the frequency band, and the mechanisms causing the falloff of gain at the band edges were identified. It was found that the second-harmonic circuit resonance is crucial in determining amplifier performance. By examining the dependence of bandwidth on the location and steepness of this resonance, an estimate was made of the maximum obtainable bandwidth for a TRAPATT amplifier, using a slug-tuned coaxial circuit and fundamental extraction.

References

[1] P. E. Bauhahn, "Properties of semiconductor materials and microwave transit-time devices," Ph.D. dissertation, The University of Michigan, Ann Arbor, MI, Oct. 1977.

[2] T. T. Fong and R. S. Ying, "Solid state amplifier for spread spectrum communications," Hughes Research Labs., Torrance, CA, Final Tech. Rep. No. RADC-TR-75-56, Feb. 1975.

[3] H. J. Prager, K. K. N. Chang, and S. Weisbrod, "High-power high-efficiency silicon avalanche diodes at ultra high frequencies," *Proc. IEEE* (Corres.), vol. 55, pp. 586–587, Apr. 1967.

[4] H. J. Prager, K. K. N. Chang, and S. Weisbrod, "Power amplification with anomalous avalanche diodes," *IEEE Trans. Microwave Theory Tech.*, vol. MTT-18, pp. 956–963, Nov. 1970.

[5] H. Kawamoto, S. G. Liu, H. J. Prager, and E. L. Allen, "*S*-band TRAPATT amplifiers with four-layer diode structures," *RCA Rev.*, vol. 35, pp. 372–386, Sept. 1974.

[6] A. Rosen, H. Kawamoto, J. Klatskin, and E. L. Allen, "Integrated TRAPATT diode arrays," *IEEE Trans. Microwave Theory Tech.*, vol. MTT-23, pp. 841–843, Oct. 1975.

[7] H. Kroger and M. I. Grace, "TRAPATT amplifier," Sperry Rand Res. Center, Sudbury, MA, Final Rep. No. RADC-TR-74-261, Jan. 1975.

[8] J. P. Quine, "Circuit behavior and impedance characteristics of broad-band TRAPATT-mode amplifiers," *IEEE Trans. Microwave Theory Tech.*, vol. MTT-27, pp. 23–31, Jan. 1979.

[9] M. Khochnevis-Rad, "Transient analysis of the TRAPATT mode of oscillation," Ph.D. dissertation, The University of Michigan, Ann Arbor, MI, Aug. 1977.

[10] S. P. Chan, S. Y. Chan, and S. G. Chan, *Analysis of Linear Networks and Systems*. Reading, MA: Addison Wesley, 1972.

[11] A. Rosen, H. Kawamoto, H. J. Prager, S. G. Liu, and R. W. Paglione, "*S*-band amplifier-TRAPATT," RCA Lab., Rep. No. ECOM-72-0213, Princeton, NJ, 1974.